Functional coupling of pontine waves and hippocampal sharp wave-ripples during NREM sleep

Abbreviated title: P-waves and hippocampal oscillations across sleep

Tomomi Tsunematsu[1,2], Sumire Matsumoto[2,4], Mirna Merkler[3,4], and Shuzo Sakata[3]

[1] Department of Integrative Life Sciences, Graduate School of Life Sciences, Tohoku University, Sendai 980-8577, Japan

[2] Frontier Research Institute for Interdisciplinary Sciences, Tohoku University, Sendai 980-8578, Japan

[3] Strathclyde Institute of Pharmacy and Biomedical Sciences, University of Strathclyde, 161 Cathedral Street, Glasgow G4 0RE, UK

[4] Equal contribution

Correspondence should be addressed to S. Sakata (shuzo.sakata@strath.ac.uk)

Acknowledgements

We thank Dr Tomomi Sanagi, Dr Amisha Patel and Jacques Ferreira for technical assistance. This work was supported by Leverhulme Trust (RPG-2015-377), MRC (MR/V033964/1) and Horizon2020-RIA (DEEPER, 101016787) to SS, and by the Japan Society for the Promotion of Science (JSPS) Postdoctoral Fellow for Research Abroad, a Research Fellowship from the Uehara Memorial Foundation, FOREST (JPMJFR2047) from Japan Science and Technology Agency and JSPS KAKENHI (20H05047) to TT.

Author contributions

TT and SM performed all *in vivo* electrophysiological experiments and associated histological analysis and sleep scoring. MM performed all Neuropixels probe experiments and pre-processing. SS performed all other data analysis. SS wrote the manuscript with inputs from TT, SM and MM.

Conflict of interest

The authors declare no competing financial interests.

Abstract

Ponto-geniculo-occipital (PGO) or pontine (P) waves have long been recognized as an electrophysiological signature of rapid eye movement (REM) sleep. However, P-waves can be observed not just during REM sleep, but also during non-REM (NREM) sleep. Recent studies have uncovered that P-waves are functionally coupled with hippocampal sharp wave-ripples (SWRs) during NREM sleep. However, it remains unclear to what extent P-waves during NREM sleep share their characteristics with P-waves during REM sleep and how the functional coupling to P-waves modulates SWRs. Here, we address these issues by performing multiple types of electrophysiological recordings and fiber photometry in both sexes of mice. P-waves during NREM sleep share their waveform shapes and local neural ensemble dynamics at a short (~100 ms) timescale with their REM sleep counterparts. However, the dynamics of mesopontine cholinergic neurons are distinct at a longer (~10 s) timescale: although P-waves are accompanied by cholinergic transients, the cholinergic tone gradually reduces before P-wave genesis during NREM sleep. While P-waves are coupled to hippocampal theta rhythms during REM sleep, P-waves during NREM sleep are accompanied by a rapid reduction in hippocampal ripple power. SWRs coupled with P-waves are short-lived and hippocampal neural firing is also reduced after P-waves. These results suggest that P-waves play distinct roles in memory consolidation by functionally coupling with hippocampal ensembles in a state-dependent manner.

Keywords: REM sleep, NREM sleep, PGO wave, Sharp wave-ripples, Theta rhythms

Significance Statement

While sleep states can be defined based on distinct electrophysiological markers, pontine (P) waves have long been recognized as a hallmark of rapid eye movement (REM) sleep. Despite their prominence, P-waves have been studied less compared to other sleep-related neural events. We still know little about the functional relationship between P-waves and other neural events across sleep states. In the present study, we discovered an unexpected relationship between P-waves and hippocampal sharp wave-ripples (SWRs) during non-REM (NREM) sleep. While P-waves and SWRs are temporally coupled, P-waves have a diminishing effect on SWRs. Because SWRs are known to play a critical role in memory consolidation, P-waves may also play a role in memory consolidation but in a sleep-state-dependent manner.

Introduction

Sleep is a fundamental homeostatic process in the animal kingdom. Determining its characteristics and exploring its functions is essential in neuroscience. Sleep states in mammals can be determined by multiple electrophysiological markers. For example, in addition to low muscle tone, cortical electroencephalograms (EEGs) during NREM sleep are characterized by slow and delta (<4 Hz) oscillations. Additionally, other oscillations including sleep spindles and hippocampal sharp wave-ripples (SWRs) have been extensively studied (Steriade et al., 1993; Steriade, 2006; Brown et al., 2012; Buzsaki, 2015; Adamantidis et al., 2019; Byron et al., 2021).

While theta (~7 Hz) oscillations are prominent during REM sleep, ponto-geniculo-occipital (PGO) waves have long been recognized (Jouvet et al., 1959; Bizzi and Brooks, 1963a; Brooks and Bizzi, 1963; Callaway et al., 1987; Datta, 1997): PGO waves during REM sleep were initially reported in cats (Bizzi and Brooks, 1963b). Subsequently, similar sub-second brain waves have been observed in other mammalian species, including rats (Farber et al., 1980; Datta, 1997), mice (Patel et al., 2020; Tsunematsu et al., 2020), macaques (Cohen and Feldman, 1968; Ramirez-Villegas et al., 2021) and humans (Lim et al., 2007). In rats, PGO waves are often called pontine-waves or “P-waves” (Datta, 2012).

P-waves consist of ~100 ms waves originating from mesopontine cholinergic nuclei, such as the pontine tegmental nucleus, laterodorsal tegmental nucleus and sublaterodorsal nucleus in rodents (Datta, 1997; Datta et al., 1998; Patel et al., 2020; Tsunematsu et al., 2020), which play an imperative role in REM sleep induction (Lu et al., 2006; Luppi et al., 2006; McCarley, 2007; Van Dort et al., 2015; Herice et al., 2019). P-waves can be observed across a wide range of brain regions, not just the visual pathway, but also in limbic areas (Calvo and Fernandez-Guardiola, 1984) and the cerebellum (Jouvet et al., 1965; Torres-Herraez et al., 2022).

During REM sleep, P-waves and hippocampal theta oscillations are coupled (Sakai et al., 1973; Karashima et al., 2002; Tsunematsu et al., 2020; Ramirez-Villegas et al., 2021): the timing of P-waves is locked to a certain phase of ongoing theta oscillations. While this was originally discovered in cats (Sakai et al., 1973; Karashima et al., 2002), recent studies confirmed a similar phase-coupling in mice (Tsunematsu et al., 2020) and macaques (Ramirez-Villegas et al., 2021). P-waves can also be observed during NREM sleep although the frequency of P-waves is less (Tsunematsu et al., 2020; Ramirez-Villegas et al., 2021). Intriguingly, recent two studies reported that P-waves during NREM sleep are coupled with hippocampal SWRs, implying a role in systems memory consolidation (Tsunematsu et al., 2020; Ramirez-Villegas et al., 2021).

Although these results suggest brain-wide coordination of sleep-related neural events across sleep states, the following issues remain unsolved. First, how similar and different are P-waves during NREM sleep compared to those during REM sleep? While the detection of P-waves relies on local

field potentials, the underlying neural dynamics may be different. However, no previous studies have addressed this issue directly. Second, it remains to be determined what is the consequence of the functional coupling between SWRs and P-waves with respect to hippocampal ensembles. Because the duration of SWRs is a critical factor for memory consolidation (Fernandez-Ruiz et al., 2019), it is important to determine how the duration of SWRs and the excitability of hippocampal neurons are influenced by P-waves. In the present study, by analyzing our published datasets (Patel et al., 2020; Tsunematsu et al., 2020) and performing additional electrophysiological and fiber photometry experiments in mice, we report that although brainstem neural activity associated with P-waves is similar between two sleep states, mesopontine cholinergic activity exhibits distinct dynamics at a long (~10 s) timescale. We also uncover a non-trivial antagonistic role of P-waves with SWRs, suggesting the functional importance of P-waves in systems memory consolidation.

Materials and Methods

Animals

24 mice (8-37 weeks old, 19 males, 5 females) were used in this study and were housed individually with a 12 h:12 h light/dark cycle (light on hours: 7:00-19:00 for 22 mice, 8:00-20:00 for 2 mice). Mice had *ad libitum* access to food and water. Their genotypes consisted of wild-type, ChAT-IRES-Cre (JAX006410), or ChAT-IRES-Cre::Ai32 (JAX012569) on a C57BL/6 background. For brainstem silicon probe recordings, 7 animals were used (9 recordings). For hippocampal silicon probe recordings, 2 animals were used (4 recordings). For hippocampal Neuropixels probe recordings, 3 animals were used (3 recordings). For P-wave recordings with bipolar electrodes, 8 animals were used (15 recording sessions with 9 bilateral recordings). For photometry recordings, 4 animals were used (8 recordings). All experiments were performed during the light period (zeitgeber time (ZT) 1-10). All experimental procedures were performed in accordance with the United Kingdom Animals (Scientific Procedures) Act of 1986 Home Office regulations and approved by the Home Office (PPL 70/8883) and the Animal Care and Use Committee of Tohoku University (approval no. 2019LsA-018). While the majority of the datasets were taken from previous studies (Patel et al., 2020; Tsunematsu et al., 2020), the following datasets were added for the present study: 4 recordings for bilateral P-wave recordings; 3 recordings for Neuropixels probe recordings; 2 recordings for photometry recordings.

Surgical procedures

Detailed procedures were described elsewhere (Tsunematsu et al., 2020). Briefly, mice were anesthetized with isoflurane (2-5% for induction, 1-2% for maintenance) and placed in a stereotaxic apparatus (SR-5M-HT or SR-6M-HT, Narishige). Body temperature was maintained at 37°C with a feedback temperature controller (40–90–8C, FHC). After exposing the skull, two bone screws were implanted on the skull for cortical EEGs. Twisted wires (AS633, Cooner Wire) were inserted into the neck muscle for EMG. For pontine EEG recording, bipolar electrodes for pontine EEGs were typically implanted in the medial parabrachial nucleus of the pons (5.1 mm posterior, 1.2 mm lateral from bregma, 3.2 mm depth from brain surface) or the sublaterodorsal nucleus (5.1 mm posterior, 0.6 mm lateral from bregma, 2.6 mm depth from brain surface). The bipolar electrodes consisted of 75 or 100 µm diameter stainless wires (FE631309, Advent Research Materials; FE205850, Goodfellow; EKCSS-010, Bio Research Center). The tips of two glued wires were separated by approximately 0.5 mm vertically to differentiate signals. A pair of nuts was also attached on the skull with dental cement as a head-post. After the surgery, Carprofen (Rimadyl, 5 mg/kg) was administered intraperitoneally. The animals were left to recover for at least 5 days. During the habituation period, the animals were placed in a head-fixed apparatus, by securing them by the head-post and placing the animal into an acrylic tube. This procedure was continued for at least 5 days, during which the

duration of head-fixed was gradually extended from 10 to 120 min. After this period, a recording was performed for up to 5 hours (see below).

For silicon probe or Neuropixels probe recording, in addition to the procedures above, a day after the habituation period, the animals were anesthetized with isoflurane and a craniotomy to insert a probe into the brainstem or hippocampus was performed. A craniotomy on the left hemisphere (4.0 mm to 5.5 mm posterior, 1.0 to 1.3 mm lateral from bregma) for the brainstem recording or on the left hemisphere (2.0 mm posterior, 1.5 mm lateral from bregma or 2.5 to 3.5 mm posterior, 2.4 to 3.4 mm lateral from bregma) for the hippocampus recording were performed, respectively. To protect and prevent the brain from drying, the surface was covered with biocompatible sealants (Kwik-Sil and Kwik-Cast, WPI). The following day, the animals were placed in the head-fixed apparatus for recording.

For simultaneous in vivo electrophysiology and fiber photometry (Patel et al., 2020), the viral vector (AAV5-CAG-flex-GCaMP6s-WPRE-SV40, Penn Vector Corel titer 8.3 x 10^{12} GC/ml) was injected in the pedunculopontine tegmental nucleus (PPN) and laterodorsal tegmental nucleus (LDT) (-4.5 mm posterior, 1.m mm lateral from bregma, 3.25 mm depth from brain surface). A hybrid implant consisting of a bipolar electrode glued to an optic fiber was implanted 3 mm deep from the brain surface in addition to bone screws for cortical EEGs and twisted wires for EMG. All components were fixed with dental cement.

in vivo electrophysiological recording

Electrophysiological recordings were performed in a single-walled acoustic chamber (MAC-3, IAC Acoustics) with the interior covered with 3 inches of acoustic absorption foam. The animals were placed in the same head-fixed apparatus, by securing them by the head-post and placing the animal into an acrylic tube. During the entire recording, the animals were not required to do anything actively. For pontine EEG recording, cortical EEG, EMG and pontine EEG signals were amplified (HST/32V-G20 and PBX3, Plexon), filtered (0.1 Hz low cut), digitized at a sampling rate of 1 kHz and recorded using LabVIEW software (National Instruments). A subset of recordings was performed using an Intan Technologies system (RHD 16-channel bipolar-input recording headstage, RHD2000). The recording was performed for approximately 5 hrs between ZT1-6.

For silicon probe recording, a 32-channel 4-shank silicon probe (A4 x 8-5 mm-100-400-177 for brainstem recording or Buzsaki32 for hippocampus recording) was inserted slowly with a manual micromanipulator (SM-25A, Narishige) into the brainstem (3.75 mm – 4.3 mm from the brain surface) or the hippocampus (1.55 mm – 1.85 mm from brain surface). Broadband signals were amplified (HST/32V-G20 and PBX3, Plexon) relative to a screw on the cerebellum, filtered (0.1 Hz low cut), digitized at 20 kHz and recorded using LabVIEW software (National Instruments). For Neuropixels

probe recording, the probe was inserted slowly with a motorized manipulator (DMA-1511, Narishige) through the hippocampus (4 mm from the brain surface). Signals were amplified and digitized in the probe and recorded using SpikeGLX (Janelia Research Campus). The recording session was initiated > 1 hr after the probe was inserted into its target depth, to stabilize neural signals. For verification of probe tracks, the rear of the probe was painted with DiI (~10% in ethanol, D282, Invitrogen) or CM-DiI (0.1% w/v in ethanol, C7001, Invitrogen) before insertion. Pupillometry was also measured simultaneously from a subset of recordings. The experimental procedures and results of pupillometry were reported elsewhere (Tsunematsu et al., 2020).

Simultaneous in vivo electrophysiology and fiber photometry

Detailed procedures were described elsewhere (Patel et al., 2020; Tsunematsu et al., 2020). Briefly, recordings were performed in an open box (21.5 cm x 47 cm x 20 cm depth) lined with absorbent paper, bedding, and soft food. Electrophysiological signals were recorded at 1 kHz using an interface board (RHD2000, Intan Technologies) and connected to the mouse via an amplifier (RHD2132, Intan Technologies). The fiber photometry system consisted of two excitation channels: a 470 nm LED for Ca^{2+}-dependent signals and a 405 nm LED for Ca^{2+}-independent isosbestic signals. LED pulses were alternately turned on and off at 40 Hz. The illumination power was adjusted at the tip of the fiber to 0.7-1.37 mW/mm^2 for the 470 nm LED and 0.4-0.94 mW/mm^2 for the 405 nm LED. Emission signals were collected back through the optic fiber and directed to a photodetector (NewFocus2151, Newport). A data acquisition module (NI USB-6211, National Instruments) and a custom-written program (LabVIEW) were used to control the LEDs and acquire both fluorescence signals and electrophysiological signals at 1 kHz.

Histological analysis

After electrophysiological experiments, animals were deeply anesthetized with a mixture of pentobarbital and lidocaine and perfused transcardially with saline or phosphate buffer saline (PBS) followed by 4% paraformaldehyde/0.1 M phosphate buffer, pH 7.4. The brains were removed and immersed in the above fixative solution overnight at 4°C and then immersed in 30% sucrose in PBS for at least 2 days. The brains were cut into coronal or sagittal sections with a sliding microtome (SM2010R, Leica) or with a cryostat (CM3050, Leica) with a thickness of 50 or 100 µm. To identify the location of electrode positions, the brain sections were incubated with NeuroTrace 500/525 Green-Fluorescence (1/350, Invitrogen), NeuroTrace 435/455 Blue-Fluorescence (1/100, Invitrogen) or DAPI (1/1000, Invitrogen) in PBS for 20 min at room temperature (RT). After staining, sections were mounted on gelatin-coated or MAS-coated slides and cover-slipped with 50% glycerol in PBS. The sections were examined with a fluorescence microscope (BZ-9000, Keyence). For Neuropixels probe experiments, the track of the probe was estimated using publicly available software (https://github.com/cortex-lab/allenCCF).

Data analysis

Sleep scoring

Vigilance states were visually scored offline according to standard criteria as described elsewhere (Patel et al., 2020; Tsunematsu et al., 2020). Wakefulness, NREM sleep, or REM sleep were determined every 4 seconds based on cortical EEG and EMG signals using a custom-made MATLAB GUI (https://github.com/Sakata-Lab/SleepScore) or SleepSign (KISSEI COMTEC).

Photometry signal processing

Detailed procedures were described elsewhere (Patel et al., 2020). Briefly, the median fluorescent signals during each LED pulse were calculated, meaning that the original signals were effectively down-sampled to 40 Hz. Photobleaching was estimated by fitting a single exponential curve and the fluorescent signals were subtracted from the estimate. After applying a low-pass (<4 Hz) filter, the 405 nm signals were scaled based on the 470 nm signals using linear regression. Finally, the 470 nm signals were subtracted from the scaled 405 nm signals.

P-wave detection

To detect P-waves, two EEG or LFP signals in the pons were subtracted and filtered (5-30 Hz band-pass filter). If the signals cross a threshold, the event was considered to be a P-wave candidate. To determine the detection threshold, a segment of signals was extracted from the longest NREM sleep episode for a reliable estimation of the noise level. The noise level was estimated by computing root-mean-square (RMS) values in every 10 ms window. The threshold was defined as the mean + 5 x standard deviation of the RMS values. To eliminate potential moving artifacts, EMG signals were also assessed in parallel. If the RMS values of EMG signals cross a threshold, the candidate was discarded. The threshold was defined as the mean + 3 × standard deviation (SD) of the RMS values of EMG signals with 10 ms resolution. The timing of P-waves was defined as the timing of the negative peak.

SWR detection

To detect ripples in the hippocampus, LFP signals in CA1 were band-pass filtered at 80-250 Hz with a 3rd-order Butterworth filter. The envelope of the filtered signals was calculated by computing root-mean-square values using a sliding window of 20-ms data points. The mean and SD of this “ripple” power profile were used to compute two thresholds (mean + 5×SD and mean + 2×SD), which were used to detect SWRs and to determine their onset, peak timing and offset. To detect SWRs, the period of the ripple power larger than the threshold (mean + 5×SD) was recognized as SWR candidates. The peak timing of each candidate was defined as SWR timing. The onset and offset of

each candidate were determined as time points when the candidate's power profile crossed the threshold (mean + 2×SD). If the onset and offset were overlapped across multiple SWR candidates, they were merged as a single SWR and the SWR timing was defined as the time point providing the maximum power. Finally, candidates shorter than 20 ms or longer than 200 ms were excluded. This process was applied to all silicon probe channels. Signals from the channel which provided the highest frequency of SWRs during NREM sleep, but low frequency of SWRs during REM sleep was used. In Neuropixels probe recording, the position of the CA1 pyramidal cell layer was estimated by computing the ratio between SWR frequency during NREM and REM sleep. The channel that showed the maximum value was chosen.

Phase and band power analysis

The phase analysis (**Fig. 4B**) was the same as that described previously (Yague et al., 2017; Tsunematsu et al., 2020). LFP signals from two separate channels were subtracted to minimize volume conduction. To derive band-limited signals at theta band (7 – 10 Hz), a Kaiser finite impulse response filter with sharp transition bandwidth of 1 Hz, pass-band ripple of 0.01 dB and stop-band attenuation of 50 dB. For filtering, MATLAB *filtfilt* function was used. The instantaneous phase of the theta band was estimated from the Hilbert transform and the phase of P-wave occurrence was computed. To quantify the relationship between P-waves and LFP phase, the number of P-waves elicited in each phase bin was calculated. The resultant vector length was computed as an absolute value of the mean resultant vector r by using *circ_r* function of CircStats Toolbox (Berens, 2009). Rayleigh's test for non-uniformity of circular data was performed to assess the statistical significance ($p < 0.01$) of the non-uniformity of the P-wave vs LFP phase distribution.

To estimate theta powers (**Fig. 4C**), band-limited signals at theta band (7 – 10 Hz) were used. To estimate ripple powers (**Fig. 4E**), band-limited signals were derived at 80 – 250 Hz. Then, those signals were cross-correlated with P-wave timing during REM sleep for the theta band and NREM sleep for the ripple band.

Spike train analysis

For both conventional silicon probe and Neuropixels recording data, Kilosort (Pachitariu et al., 2016) was used for automatic processing, followed by manual curation using phy (https://github.com/cortex-lab/phy). Clusters with ≥20 isolation distance were recognized as single units. The position of recorded neurons was estimated based on histological analysis. This estimation was refined by computing the ratio of SWR frequency between NREM and REM sleep (the channel exhibiting the highest ratio was set as the CA1 pyramidal layer). In the present study, we analyzed only CA1 neurons. All subsequent analyses were performed using custom-written codes (MATLAB, Mathworks).

Statistical analysis

Data were presented as mean ± SEM unless otherwise stated. Statistical analyses were performed with MATLAB. In **Figures 2A, 2B** and **4F**, Wilcoxon rank sum test was performed. In **Figure 2D**, Pearson's cross-correlation analysis was performed. In **Figures 3B, 4E** and **4H**, Student's *t*-test was performed.

Results

P-waves during NREM and REM sleep

We performed three types of electrophysiological recordings: firstly, we performed pontine EEG recording to detect P-waves by chronically implanting a bipolar electrode (*n* = 11 sessions from 6 animals) (**Fig. 1A**). Secondly, we performed silicon probe recording in mid-hindbrain regions (we call it as the "brainstem" afterward) to monitor spiking activity associated with P-waves (*n* = 9 sessions from 7 animals) (**Fig. 1D**). Finally, we performed conventional silicon or Neuropixels probe recording in the hippocampal CA1 while monitoring pontine EEGs to investigate the relationship between P-waves and hippocampal oscillations (*n* = 7 sessions from 5 animals) (**Fig. 4A**). Across all experiments, we also monitored cortical EEGs and electromyograms (EMGs) to determine sleep states. While we carried out all experiments in a head-fixed condition since we combined silicon probe recording and pupillometry, the sleep architecture was generally comparable with that in a tethered unrestrained condition as reported previously (Tsunematsu et al., 2020).

In all recording sessions where we could confirm REM sleep, we observed P-waves (**Figs. 1C and E**). The position of electrodes was histologically confirmed in the mesopontine region (**Fig. 1B**). P-waves often appeared as a cluster during REM sleep whereas P-waves during NREM sleep appeared less, typically in isolation (**Fig. 1C**). P-waves during both sleep states were accompanied by spiking activity across simultaneously recorded brainstem neurons (**Fig. 1E**), indicating that P-waves were locally generated neural events, rather than artifacts due to volume conduction or other electrical events. Thus, we could confirm P-waves in mice.

Since we also detected P-waves during NREM sleep, not just during REM sleep, we assessed whether detected P-waves were comparable between NREM sleep and REM sleep (**Figs. 1F-H**). As shown in **Figure 1F**, the average waveform of P-waves was similar between states. To quantify this tendency, we applied principal component analysis (PCA) (**Fig. 1G**) and measured Pearson's correlation coefficient (**Fig. 1H**). We confirmed the large overlap of individual waveforms between NREM and REM sleep in the first 2 PC space (**Fig. 1G**) as well as the high correlation coefficient (0.977 ± 0.003) (**Fig. 1H**), indicating that detected P-waves are quantitatively similar between sleep states.

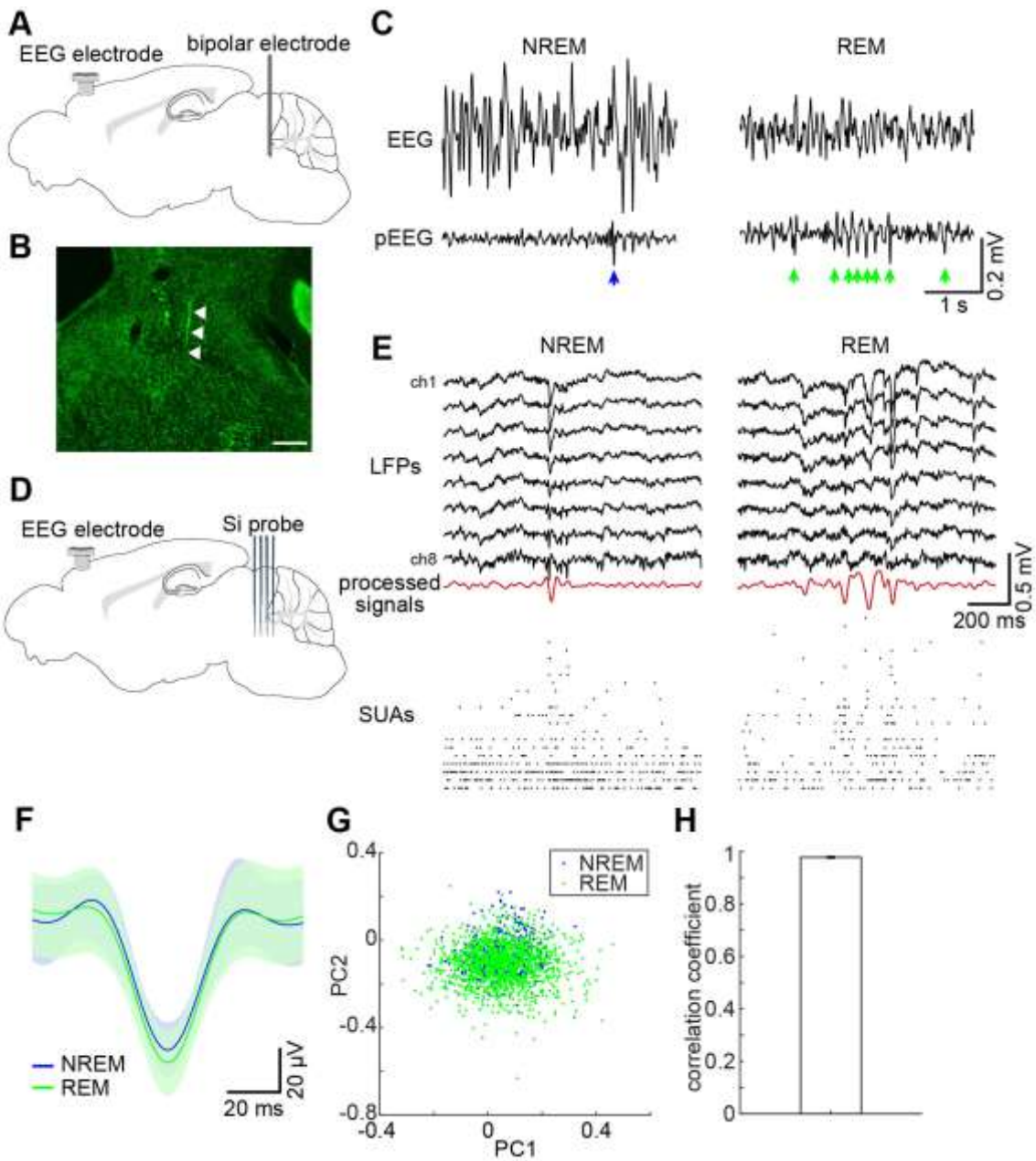

Figure 1. P-waves during NREM and REM sleep.

(**A**) A diagram of the experimental approach for P-wave recording, showing a cortical EEG electrode and a bipolar electrode for pontine EEG recording in the mouse. For EMG recording, a twisted bipolar electrode was also inserted in the neck muscle.

(**B**) A photograph showing a track of a bipolar electrode in the mesopontine region. Scale bar, 500 µm.

(**C**) Examples of P-waves during NREM (*left*) and REM sleep (*right*).

(**D**) A diagram of the experimental approach to brainstem population recording, showing a cortical EEG electrode and a 32-channel silicon probe.

(**E**) Examples of local field potentials (LFPs) and simultaneously recorded single unit activities (SUAs) during NREM (*left*) and REM sleep (*right*). Processed LFP signals for P-wave detection (red) are also shown.

(**C**) Average waveforms of P-waves. *blue*, P-waves during NREM sleep; *green*, P-waves during REM sleep. Errors indicate SD.

(**D**) Detected individual P-waves represented in first two PC (principal component) space.

(**E**) Comparisons of average waveforms of P-waves between sleep states based on Pearson's correlation coefficient (n = 16, r = 0.97 ± 0.01).

Similarity and difference in the basic properties of P-waves between sleep states

Next, we examined if the characteristics of P-waves are different between NREM and REM sleep (**Fig. 2**). We began by comparing the frequency of P-waves between sleep states (**Fig. 2A**). The frequency of P-waves during REM sleep was around 0.5 – 1 Hz, and this was significantly higher than NREM sleep (n = 38, $p < 0.0001$, rank sum test). We did not find any statistically significant difference in P-wave frequency between recording methods (bipolar electrodes v.s. silicon probes; 31 v.s. 7) ($p = 0.36$ during NREM; $p = 0.18$ during REM, rank sum test with Bonferroni correction).

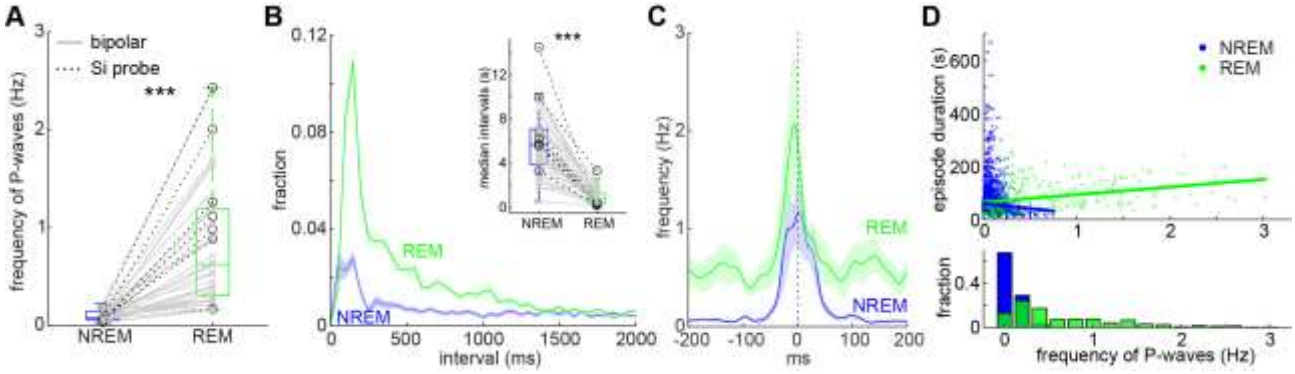

Figure 2. Features of P-waves during NREM and REM sleep.
(**A**) Comparison of P-wave frequency between sleep states. $n = 38$ recordings. *** $p < 0.0001$, rank sum test.
(**B**) Comparison of inter-P-wave intervals between sleep states. inset, comparison of the median intervals of P-waves between states. $n = 38$ recordings, *** $p < 0.0001$, rank sum test.
(**C**) Cross-correlation of bilateral P-wave timing. $n = 9$ recordings.
(**D**) The relationship between P-wave frequency and sleep episode duration. Lines are linear regression lines. *Bottom*, distributions of P-wave frequency during NREM (blue) and REM sleep (green).

Since P-waves during REM sleep often appear as clusters (**Fig. 1**), we quantified the inter-event intervals (**Fig. 2B**). As expected, a large fraction of P-waves appeared within 200 ms, especially during REM sleep. The median interval of P-waves was also significantly shorter during REM sleep (**Fig. 2B inset**) (n = 38, $p < 0.0001$, rank sum test). To examine whether P-waves can occur synchronously in two hemispheres, we took advantage of some datasets (n = 9 sessions from 5 animals) where bipolar electrodes were implanted bilaterally (**Fig. 2C**). Intriguingly, cross-correlation analysis showed the synchronous occurrence of P-waves between two hemispheres during both REM and NREM sleep. In addition, the cross-correlation profile during REM sleep exhibited a weak modulation in the 100 – 200 ms range, suggesting rhythmic theta synchrony between two hemispheres.

Because the frequency of P-waves gradually increases at around the onset of REM sleep as reported before (Tsunematsu et al., 2020), we wondered if the frequency of P-waves during REM sleep episode can correlate with the duration of REM sleep episodes (**Fig. 2D**). We found that this is the case ($r = 0.38$, $p < 0.0001$) whereas the frequency of P-waves during NREM sleep negatively correlated with episode duration ($r = -0.064$, $p < 0.005$). Altogether, although the waveform of P-waves is similar between sleep states, basic characteristics are markedly different between states.

Similarity and difference in underlying brainstem neural activity between sleep states

While P-waves consist of a large deflection of LFPs (**Fig. 1**), it remains unclear whether the underlying neural activity also consists of synchronous population firing or diverse neural activities. To address this issue, we analyzed single unit activity in the brainstem (**Fig. 3**). Indeed, many neurons exhibited the peak of their activity around P-wave timing (**Fig. 3A**). To examine whether the temporal structure of neural firing is preserved between NREM and REM sleep, we measured Pearson's correlation coefficient between activity patterns in both states across neurons (**Fig. 3B**). The mean of Pearson's correlation coefficient was significantly higher than zero ($p < 0.0001$, *t*-test). Thus, the firing pattern associated with P-waves was generally preserved at the population level between sleep states.

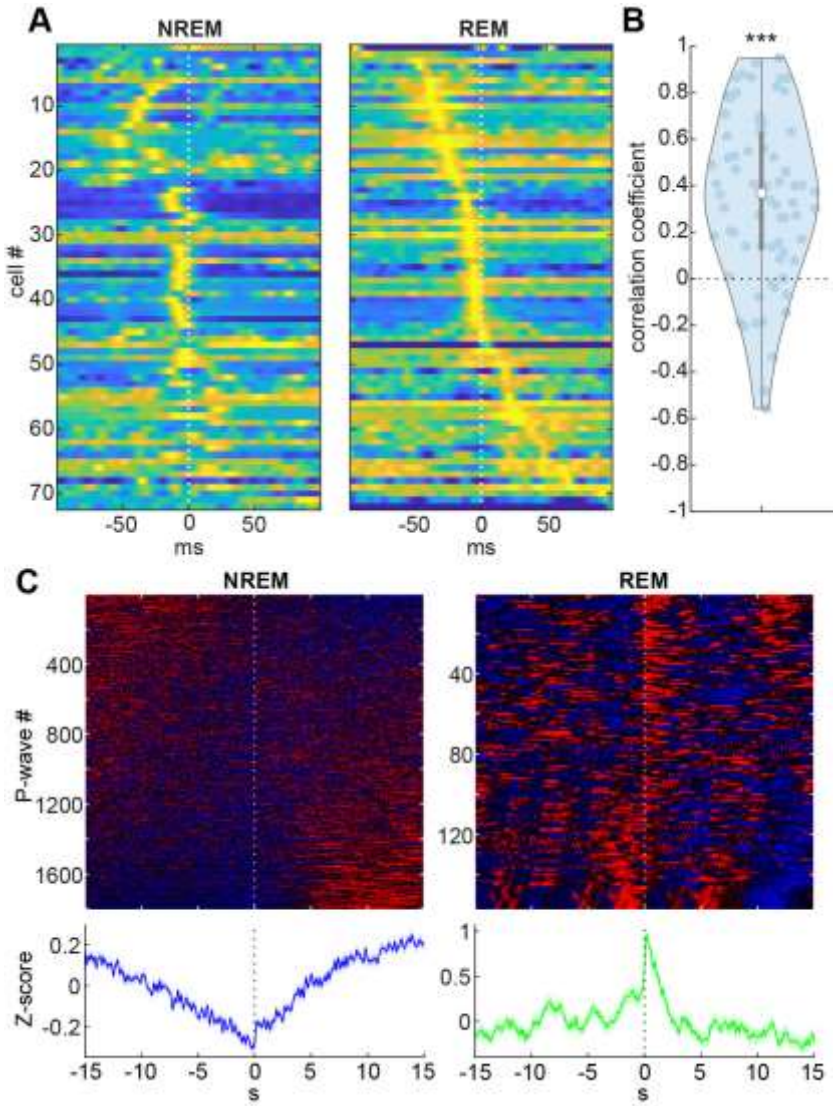

Figure 3. Brainstem neural firing associated with P-waves.
(**A**) Normalized average firing profiles across cells during NREM (*left*) and REM sleep (*right*). Cells were sorted by peak timing during REM sleep.
(**B**) Comparisons of mean firing profiles between sleep states across cells (n = 72) based on Pearson's correlation coefficient. *** $p < 0.0001$, *t*-test.
(**C**) Normalized (Z-scored) photometry signals of mesopontine cholinergic neurons associated with P-waves during NREM (*left*) and REM sleep (*right*). The top panels show individual normalized signal traces sorted by the 1st PC score. The color range is between -1.96 and 1.96 (equivalent to 0.05 *p*-value). The bottom panels show the average of the normalized signals.

Since mesopontine cholinergic neurons have been implicated in P-wave genesis (Callaway et al., 1987; Datta, 1997, 2012), we performed simultaneous electrophysiology and fiber photometry by expressing GCaMP6s in mesopontine cholinergic neurons. As we showed previously (Patel et al., 2020), P-waves were associated with the transient activity of cholinergic neurons during REM sleep (**Fig. 3C**). Interestingly,

although the transient activity of cholinergic activity was also confirmed during NREM sleep, the level of cholinergic activity gradually decreased before P-waves and increased after P-waves (**Fig. 3C**). Thus, although brainstem population activity associated with P-waves is generally similar between sleep states at a short (sub-second) timescale, at least mesopontine cholinergic neurons exhibit distinct activity patterns at a long (10s of seconds) timescale.

Functional coupling between P-waves and hippocampal theta oscillations during REM sleep

Previously we demonstrated state-dependent functional coupling between P-waves and hippocampal oscillations across sleep states (Tsunematsu et al., 2020) and similar results were reported in macaque monkeys (Ramirez-Villegas et al., 2021). However, it remains to be determined how hippocampal oscillations are modulated by coupling with P-waves across sleep states. In particular, it is unclear how sharp wave-ripples (SWRs) can be modulated by P-waves. To address these issues, we performed silicon or Neuropixels probe recording from the hippocampal CA1 while monitoring P-waves (**Fig. 4A**). Although the Neuropixels probe allows monitoring of neural activity across multiple brain regions, in this study, we focus on the CA1 since the CA1 is the source of ripples (Sullivan et al., 2011; Buzsaki, 2015; Liu et al., 2022).

Firstly, we confirmed the coupling between P-waves and hippocampal theta oscillations during REM sleep (**Figs. 4B and C**). As expected, the average LFP signals showed rhythmic modulation around P-wave onset (**Fig. 4B**). We assessed this in the frequency domain by applying a wavelet transformation (**Fig. 4B**). We confirmed that this modulation was associated with an increase in their frequency band. We also determined when P-waves appeared during each theta cycle (**Fig. 4B**). More P-waves appeared during the rising phase of theta oscillation ($p < 0.0001$, Rayleigh test for non-uniformity). We confirmed the increase in theta power across recordings (n = 7) (**Fig. 4C**). These results reassure us that P-waves are coupled to hippocampal theta oscillations during REM sleep.

Diminishing effects of P-waves on hippocampal SWRs during NREM sleep

Next, we examined if hippocampal SWRs coupled with P-waves have distinct features (**Figs. 4D-F**). We began by comparing the frequency of SWRs and P-waves during NREM to REM sleep transitions (**Fig. 4D**). These two neural events appeared complementary: while SWRs appeared mostly during NREM sleep, P-waves appeared more during REM sleep.

Although we previously reported that P-waves are coupled with SWRs (Tsunematsu et al., 2020), it is unclear if and how P-waves can be associated with the modulation of SWRs. To address this, we computed ripple power (80-250 Hz) around P-wave onset (**Fig. 4E**). We found that ripple power sharply increases just before the timing of P-waves, consistent with our previous finding to

demonstrate the coupling between SWRs and P-waves. However, ripple power rapidly decreased immediately after P-wave timing. This observation was confirmed across recordings (n = 9) by computing the asymmetry index that quantifies the difference in ripple power in a 250-ms window before and after P-waves (**Fig. 4E *inset***). These results imply that the occurrence of P-waves may lead to the termination of SWRs.

To test this prediction, we compared the duration of SWRs depending on whether P-waves were coupled with SWRs in a short time window. While the fraction of SWRs coupled with P-waves within 30 ms was limited (0.6 ± 0.3 % of all SWRs during NREM sleep; 2.3 ± 0.9 % of all P-waves during NREM sleep, n = 7 recordings), we found that these SWRs coupled with P-waves were significantly shorter than the remaining SWRs (**Fig. 4F**) ($p < 0.0001$, rank sum test). This tendency was confirmed within a 60 ms window. We further examined whether CA1 neural activity is modulated by P-waves (**Fig. 4G**). A group of neurons showed strong modulation at around the timing of P-waves: a subset showed a reduction in their firing after P-waves (**Fig. 4G**). To quantify this observation, we computed the normalized difference in firing rate before and after P-waves as the modulation index (**Fig. 4H**). Overall CA1 neural firing was significantly reduced after P-waves during NREM sleep ($p < 0.001$, *t*-test). These results suggest that P-waves are functionally coupled to hippocampal oscillations in a sleep-state-dependent fashion. We uncovered the non-trivial relationship between P-waves and SWRs during NREM sleep.

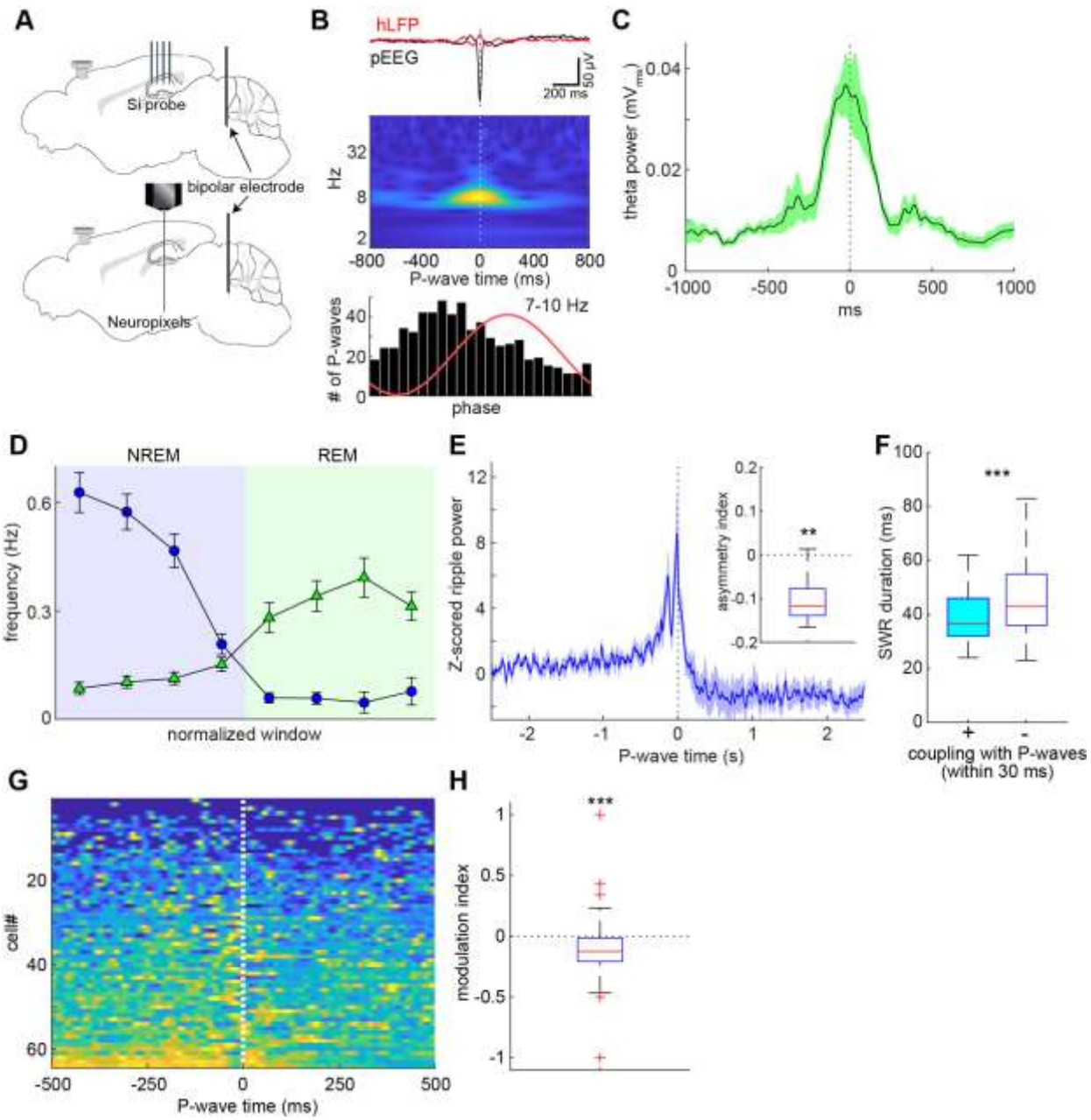

Figure 4. Functional coupling between P-waves and hippocampal oscillations during REM and NREM sleep.

(**A**) A diagram of the experimental approach to hippocampal population recording.

(**B**) *top*, the average hippocampal LFPs triggered by P-wave timing. *middle*, a scalogram of P-wave-triggered hippocampal LFPs. *bottom*, a phase diagram of P-wave timing relative to hippocampal theta rhythms.

(**C**) The average of hippocampal theta (7-10 Hz) power relative to P-wave timing. Event-triggered theta power was computed across recordings (n = 7).

(**D**) Temporal profiles of SWRs (blue) and P-waves (green) across NREM and REM sleep episodes. Each episode duration was divided into four discrete time bins as normalized time windows.

(**E**) Cross-correlation between the ripple power (80-250 Hz) profile and P-waves during NREM sleep. Each cross-correlation profile was z-scored based on the profile in a -3~-2 sec window. *Inset*, the asymmetry index, a normalized difference in the normalized ripple power before and after P-wave timing in a 250 ms window. The negative value indicates the lower ripple power after P-waves. ** $p < 0.005$, *t*-test. n = 7.

(**F**) Comparison of SWR duration between SWRs coupled with P-waves within 30 ms (n = 84) and other SWRs (n = 16689). *** $p < 0.001$, rank sum test.

(**G**) Mean activity profiles of CA1 neurons (n = 65) relative to P-wave timing during NREM sleep. Cells were sorted by their first principal component score.

(**H**) The modulation index, a normalized difference in firing rate before and after P-waves. *** $p < 0.001$, *t*-test.

Discussion

Although P-waves have long been recognized as a signature of REM sleep, P-waves can also be observed during NREM sleep. However, the detailed characteristics and functional significance of P-waves during both sleep states remain poorly understood. Here, by performing multiple types of *in vivo* electrophysiological experiments and fiber photometry in mice, we described the similarity and difference in P-waves between sleep states in mice. Novel observations can be summarized as follows: first, P-waves appear synchronously in both hemispheres (**Fig. 2C**). Second, while brainstem neural firing patterns associated with P-waves are generally similar between sleep states at a short timescale, mesopontine cholinergic activity shows distinct dynamics between sleep states at a longer timescale (**Fig. 3**). Finally, we found that SWRs coupled with P-waves are short-lived (**Fig. 4**). These results suggest that P-waves are part of state-dependent, brain-wide neural ensembles during sleep and P-waves may contribute to memory consolidation in a sleep state-dependent manner by functionally coupling to hippocampal oscillations.

Comparisons with previous studies

P/PGO waves have been described in multiple mammalian species, including cats (Jouvet et al., 1959; Bizzi and Brooks, 1963b; Brooks and Bizzi, 1963; Datta, 1997), macaques (Cohen and Feldman, 1968; Ramirez-Villegas et al., 2021), rats (Farber et al., 1980) and humans (Lim et al., 2007). However, the existence of P-waves in mice has been anecdotal despite the importance of the animal model. While we recently showed P-waves in mice directly by using electrophysiological methods and indirectly by applying fiber photometry (Patel et al., 2020; Tsunematsu et al., 2020), the characteristics of P-waves during NREM sleep were unclear.

P-waves in mice are similar to those in other species, with respect to the following features. First, the waveform of P-waves in mice (**Figs. 1C and 2C**) is similar to that of other species (Datta, 1997). In the present study, we quantitatively confirmed that the waveform of P-waves is comparable between REM and NREM sleep. Second, the temporal dynamics of P-waves in mice are also comparable with those in other species (Datta, 1997), with respect to the higher frequency of P-waves during REM sleep and a gradual increase in P-wave frequency around REM sleep onset.

In addition to these, we confirmed that P-waves are functionally coupled with SWRs and theta oscillations. A similar functional coupling between the hippocampus and cerebellum has been reported recently (Torres-Herraez et al., 2022) although it remains to be confirmed if the neural events in the cerebellum are P-waves or not. More importantly, even macaque monkeys exhibit similar functional coupling (Ramirez-Villegas et al., 2021). These results suggest that P/PGO waves are part of brain-wide neural ensembles across sleep states and sleep state-dependent functional coupling between P-waves and hippocampal oscillations is evolutionally preserved.

In the present study, we reported three non-trivial observations: first, P-waves appear synchronously in both hemispheres, implying an induction mechanism of P-waves (see below). Second, we showed that although P-waves are accompanied by mesopontine cholinergic activity during both sleep states, its dynamics at a long (over seconds) timescale is state-dependent: during NREM sleep, cholinergic activity gradually decreases before P-waves whereas cholinergic activity is at peak during P-wave genesis during REM sleep. Finally, although P-waves are functionally coupled with SWRs during NREM sleep, the occurrence of P-waves was associated with a reduction in ripple power as well as CA1 neural firing. These novel observations suggest the induction mechanism of P-waves as well as the functional significance of P-waves as discussed below.

Possible mechanisms of P-wave genesis

Mesopontine cholinergic neurons have long been implicated in the induction of P/PGO waves (Datta, 1995, 1997). Indeed, mesopontine cholinergic activity is phase-locked to the onset of P-waves during both sleep states. In the present study, we showed that brainstem neural ensembles consist of diverse functional classes while activity patterns are generally consistent between sleep states (**Fig. 3A and B**), implying similar induction mechanisms of P-waves between sleep states. However, since mesopontine cholinergic neurons exhibit distinct activity at a longer timescale (**Fig. 3C**), the frequency of P-waves may be influenced by global brain-wide activities across sleep states.

In addition, P-waves appeared in both hemispheres synchronously (**Fig. 2C**). Although we do not exclude the possibility that P-waves are generated in one hemisphere first, then P-waves start to synchronize in both hemispheres, our observation provides an insightful implication for the mechanism of P-wave genesis. Because a subset of mesopontine cholinergic neurons form commissural projections (Mena-Segovia and Bolam, 2017), these neurons may play a role in the synchronization of P-waves between two hemispheres. It would be worthwhile to investigate detailed anatomical and synaptic connections within the mesopontine region between hemispheres in the future.

Functional implications of P-waves

What are the functional consequences of the state-dependent coupling of P-waves with hippocampal oscillations? Because both SWRs and theta oscillations have been implicated in systems memory consolidation (Jadhav et al., 2012; Buzsaki, 2015; Boyce et al., 2016; Fernandez-Ruiz et al., 2019), P-waves may also play a role in memory consolidation. However, given our findings (**Figs. 5 and 6**), the role of P-waves may also be state-dependent.

Although the exact role of REM sleep in systems memory consolidation remains controversial (Poe, 2017; Sara, 2017), theta oscillations during REM sleep play a causal role in memory consolidation (Boyce et al., 2016) and pharmacological manipulations of P-waves affect memory consolidation

(Datta et al., 2004). While it has long been known that P-waves are phase-coupled with ongoing theta oscillations (Sakai et al., 1973; Karashima et al., 2002; Karashima et al., 2004; Karashima et al., 2005; Tsunematsu et al., 2020; Ramirez-Villegas et al., 2021), we also confirmed that P-waves can modulate hippocampal theta power. Because REM sleep can reorganize hippocampal population activity (Grosmark et al., 2012), it would be interesting to investigate how P-waves can contribute to such a reorganization of hippocampal excitability by manipulating P-waves.

Recently it has been shown that the duration of SWRs is causally linked to the degree of memory consolidation (Fernandez-Ruiz et al., 2019). Because we showed that SWRs coupled with P-waves are shorter than other SWRs, P-waves during NREM sleep may play a modulatory role to avoid excessive activation of hippocampal populations. A plausible mechanism of the shorter SWRs could be the influence of septal cholinergic neurons (Vandecasteele et al., 2014; Zhang et al., 2021). It remains to be determined how P-waves during NREM sleep can affect the downstream activity and how experience before sleep episodes can affect this unexpected, antagonistic interaction between SWRs and P-waves.

Limitations of the study

Although our results provide insight into the functional significance of P-waves, the present study has limitations in the following aspects: first, determining the exact cell types of recorded neurons in the brainstem was challenging. This can be addressed by monitoring the activity of specific cell types with genetically encoded indicators. Second, related to the first point, although the electrode for P-wave monitoring was implanted in the medial parabrachial nucleus or nearby pontine regions, it may not have been optimal to monitor P-waves as we observed large variability in P-wave frequency across experiments (**Fig. 2A**). It would be interesting to adopt a large-scale, high-density electrode array to systematically determine the origin of P-waves. Third, although we characterized state-dependent coupling between P-waves and hippocampal oscillations, it would be critical to directly determine the functional role of these couplings by manipulating P-waves while mice perform a behavioral task before and after sleep. Despite these limitations, however, our results provide a basis for future studies toward a better understanding of the regulatory mechanisms and functions of P-waves and sleep states.

Conclusions

While P-waves appear synchronously in both hemispheres during both NREM and REM sleep, the frequency of P-waves differs between states. Underlying neural ensembles are generally consistent between states, suggesting a similar local induction mechanism with state-specific, global activity patterns on a long timescale. Because the functional coupling between P-waves and hippocampal oscillations differs between sleep states, P-waves may contribute to brain-wide neural ensembles in

a state-dependent fashion. In addition, state-dependent coupling between P-waves and hippocampal oscillations may lead to distinct consequences in their downstream neural circuits. Thus, these state-dependent coordinated activities may result in distinct functions of sleep states.

References

Adamantidis AR, Gutierrez Herrera C, Gent TC (2019) Oscillating circuitries in the sleeping brain. Nat Rev Neurosci 20:746-762.

Berens P (2009) CircStat: A Matlab Toolbox for Circular Statistics. Journal of statistical software 31:1-21.

Bizzi E, Brooks DC (1963a) Pontine reticular formation: relation to lateral geniculate nucleus during deep sleep. Science 141:270-272.

Bizzi E, Brooks DC (1963b) Functional Connections between Pontine Reticular Formation and Lateral Geniculate Nucleus during Deep Sleep. Arch Ital Biol 101:666-680.

Boyce R, Glasgow SD, Williams S, Adamantidis A (2016) Causal evidence for the role of REM sleep theta rhythm in contextual memory consolidation. Science 352:812-816.

Brooks DC, Bizzi E (1963) Brain Stem Electrical Activity during Deep Sleep. Arch Ital Biol 101:648-665.

Brown RE, Basheer R, McKenna JT, Strecker RE, McCarley RW (2012) Control of sleep and wakefulness. Physiol Rev 92:1087-1187.

Buzsaki G (2015) Hippocampal sharp wave-ripple: A cognitive biomarker for episodic memory and planning. Hippocampus 25:1073-1188.

Byron N, Semenova A, Sakata S (2021) Mutual Interactions between Brain States and Alzheimer's Disease Pathology: A Focus on Gamma and Slow Oscillations. Biology (Basel) 10.

Callaway CW, Lydic R, Baghdoyan HA, Hobson JA (1987) Pontogeniculooccipital waves: spontaneous visual system activity during rapid eye movement sleep. Cellular and molecular neurobiology 7:105-149.

Calvo JM, Fernandez-Guardiola A (1984) Phasic activity of the basolateral amygdala, cingulate gyrus, and hippocampus during REM sleep in the cat. Sleep 7:202-210.

Cohen B, Feldman M (1968) Relationship of electrical activity in pontine reticular formation and lateral geniculate body to rapid eye movements. J Neurophysiol 31:806-817.

Datta S (1995) Neuronal activity in the peribrachial area: relationship to behavioral state control. Neurosci Biobehav Rev 19:67-84.

Datta S (1997) Cellular basis of pontine ponto-geniculo-occipital wave generation and modulation. Cellular and molecular neurobiology 17:341-365.

Datta S (2012) Phasic Pontine-Wave (P-Wave) Generation: Cellular-Molecular-Network Mechanism and Functional Significance. In: Sleep and Brain Activity (Frank MG, ed), pp 147-164. San Diego: Academic Press.

Datta S, Siwek DF, Patterson EH, Cipolloni PB (1998) Localization of pontine PGO wave generation sites and their anatomical projections in the rat. Synapse 30:409-423.

Datta S, Mavanji V, Ulloor J, Patterson EH (2004) Activation of phasic pontine-wave generator prevents rapid eye movement sleep deprivation-induced learning impairment in the rat: a mechanism for sleep-dependent plasticity. J Neurosci 24:1416-1427.

Farber J, Marks GA, Roffwarg HP (1980) Rapid eye movement sleep PGO-type waves are present in the dorsal pons of the albino rat. Science 209:615-617.

Fernandez-Ruiz A, Oliva A, Fermino de Oliveira E, Rocha-Almeida F, Tingley D, Buzsaki G (2019) Long-duration hippocampal sharp wave ripples improve memory. Science 364:1082-1086.

Grosmark AD, Mizuseki K, Pastalkova E, Diba K, Buzsaki G (2012) REM sleep reorganizes hippocampal excitability. Neuron 75:1001-1007.

Herice C, Patel AA, Sakata S (2019) Circuit mechanisms and computational models of REM sleep. Neurosci Res 140:77-92.

Jadhav SP, Kemere C, German PW, Frank LM (2012) Awake hippocampal sharp-wave ripples support spatial memory. Science 336:1454-1458.

Jouvet M, Michel F, Courjon J (1959) [Electric activity of the rhinencephalon during sleep in cats]. C R Seances Soc Biol Fil 153:101-105.

Jouvet M, Jeannerod M, Delorme F (1965) [Organization of the system responsible for phase activity during paradoxal sleep]. C R Seances Soc Biol Fil 159:1599-1604.

Karashima A, Nakao M, Katayama N, Honda K (2005) Instantaneous acceleration and amplification of hippocampal theta wave coincident with phasic pontine activities during REM sleep. Brain Res 1051:50-56.

Karashima A, Nakamura K, Sato N, Nakao M, Katayama N, Yamamoto M (2002) Phase-locking of spontaneous and elicited ponto-geniculo-occipital waves is associated with acceleration of hippocampal theta waves during rapid eye movement sleep in cats. Brain Res 958:347-358.
Karashima A, Nakao M, Honda K, Iwasaki N, Katayama N, Yamamoto M (2004) Theta wave amplitude and frequency are differentially correlated with pontine waves and rapid eye movements during REM sleep in rats. Neurosci Res 50:283-289.
Lim AS, Lozano AM, Moro E, Hamani C, Hutchison WD, Dostrovsky JO, Lang AE, Wennberg RA, Murray BJ (2007) Characterization of REM-sleep associated ponto-geniculo-occipital waves in the human pons. Sleep 30:823-827.
Liu AA et al. (2022) A consensus statement on detection of hippocampal sharp wave ripples and differentiation from other fast oscillations. Nat Commun 13:6000.
Lu J, Sherman D, Devor M, Saper CB (2006) A putative flip-flop switch for control of REM sleep. Nature 441:589-594.
Luppi PH, Gervasoni D, Verret L, Goutagny R, Peyron C, Salvert D, Leger L, Fort P (2006) Paradoxical (REM) sleep genesis: the switch from an aminergic-cholinergic to a GABAergic-glutamatergic hypothesis. J Physiol Paris 100:271-283.
McCarley RW (2007) Neurobiology of REM and NREM sleep. Sleep Med 8:302-330.
Mena-Segovia J, Bolam JP (2017) Rethinking the Pedunculopontine Nucleus: From Cellular Organization to Function. Neuron 94:7-18.
Pachitariu M, Steinmetz N, Kadir S, Carandini M, Harris KD (2016) Kilosort: realtime spike-sorting for extracellular electrophysiology with hundreds of channels. BioRxiv:061481.
Patel AA, McAlinden N, Mathieson K, Sakata S (2020) Simultaneous Electrophysiology and Fiber Photometry in Freely Behaving Mice. Front Neurosci 14:148.
Poe GR (2017) Sleep Is for Forgetting. J Neurosci 37:464-473.
Ramirez-Villegas JF, Besserve M, Murayama Y, Evrard HC, Oeltermann A, Logothetis NK (2021) Coupling of hippocampal theta and ripples with pontogeniculooccipital waves. Nature 589:96-102.
Sakai K, Sano K, Iwahara S (1973) Eye movements and hipocampal theta activity in cats. Electroencephalogr Clin Neurophysiol 34:547-549.
Sara SJ (2017) Sleep to Remember. J Neurosci 37:457-463.
Steriade M (2006) Grouping of brain rhythms in corticothalamic systems. Neuroscience 137:1087-1106.
Steriade M, McCormick DA, Sejnowski TJ (1993) Thalamocortical oscillations in the sleeping and aroused brain. Science 262:679-685.
Sullivan D, Csicsvari J, Mizuseki K, Montgomery S, Diba K, Buzsaki G (2011) Relationships between hippocampal sharp waves, ripples, and fast gamma oscillation: influence of dentate and entorhinal cortical activity. J Neurosci 31:8605-8616.
Torres-Herraez A, Watson TC, Rondi-Reig L (2022) Delta oscillations coordinate intra-cerebellar and cerebello-hippocampal network dynamics during sleep. J Neurosci 42:2268-2281.
Tsunematsu T, Patel AA, Onken A, Sakata S (2020) State-dependent brainstem ensemble dynamics and their interactions with hippocampus across sleep states. Elife 9.
Van Dort CJ, Zachs DP, Kenny JD, Zheng S, Goldblum RR, Gelwan NA, Ramos DM, Nolan MA, Wang K, Weng FJ, Lin Y, Wilson MA, Brown EN (2015) Optogenetic activation of cholinergic neurons in the PPT or LDT induces REM sleep. Proc Natl Acad Sci U S A 112:584-589.
Vandecasteele M, Varga V, Berenyi A, Papp E, Bartho P, Venance L, Freund TF, Buzsaki G (2014) Optogenetic activation of septal cholinergic neurons suppresses sharp wave ripples and enhances theta oscillations in the hippocampus. Proc Natl Acad Sci U S A 111:13535-13540.
Yague JG, Tsunematsu T, Sakata S (2017) Distinct Temporal Coordination of Spontaneous Population Activity between Basal Forebrain and Auditory Cortex. Front Neural Circuits 11:64.
Zhang Y, Cao L, Varga V, Jing M, Karadas M, Li Y, Buzsaki G (2021) Cholinergic suppression of hippocampal sharp-wave ripples impairs working memory. Proc Natl Acad Sci U S A 118.